Control Engineering Practice 74 (2018) 132–143

Contents lists available at ScienceDirect

Control Engineering Practice

journal homepage: www.elsevier.com/locate/conengprac

Distributed wide-area control of power system oscillations under communication and actuation constraints

Abhishek Jain [a,*], Aranya Chakrabortty [a], Emrah Biyik [b]

[a] Electrical & Computer Engineering Department, North Carolina State University, Raleigh, United States
[b] Department of Energy Systems Engineering, Yasar University, Izmir, Turkey

ARTICLE INFO

Keywords:
Distributed control
Wide-area control
Predictive optimization
Oscillation damping
Participation factors

ABSTRACT

In this paper a distributed Model Predictive Control design is presented for inter-area oscillation damping in power systems under two critical cyber–physical constraints — namely, communication constraints that lead to sparsification of the underlying communication network, and actuation constraints that respect the saturation limits of generator controllers. In the current state-of-art, distributed controllers in power systems are executed over fixed communication topologies that are most often agnostic of the magnitude and location of the incoming disturbance signals. This often leads to a sub-optimal closed-loop performance. In contrast, the communication topology for the proposed controller is selected in real-time after a disturbance event based on event-specific correlations of the generator states with the dominant oscillation modes that are excited by that event. Since these correlations can differ from one event to another, so can the choice of the communication topology. These correlations are used to identify the most important sets of generators that must exchange state information for enhancing closed-loop damping of the inter-area modal frequencies. Effectiveness of this strategy is shown via simulations on the 48-machine, 140-bus model for the Northeast Power Coordinating Council.

1. Introduction

Over the past decade, significant increase in transmission expansion and renewable integration in the US power grid have forced power system operators to look beyond the traditional mindset of controlling the grid using local control methods, and transition to wide-area control (WAC) using synchronized phasor measurements available from Phasor Measurement Units (PMUs). One of the most commonly known application of WAC is to improve damping of power flow oscillations in small-signal models of power systems by employing state exchange between distant generators through a wide-area communication network. An enormous literature already exists for damping control of synchronous generators (Boukarim, Wang, Chow, Taranto, & Martins, 2000; Larsen, Sanchez-Gasca, & Chow, 1995; Noroozian, Ghandhari, Andersson, Gronquist, & Hiskens, 2001) using local output feedback via power system stabilizers (PSS) and FACTS devices. These controllers are known to damp fast oscillation modes quite satisfactorily, but they often fail to improve the damping of low-frequency inter-area oscillations (Jain, Biyik, & Chakrabortty, 2015). Recent papers such as (Chakrabortty & Khargonekar, 2013; Chaudhuri & Pal, 2004; Dörfler, Jovanovic, Chertkov, & Bullo, 2014) have shown that WAC can be a promising solution to this problem.

Ideally, WACs can be designed using standard pole placement techniques and state-feedback controllers such as linear quadratic regulators (LQR) (Zolotas, Chaudhuri, Jaimoukha, & Korba, 2007) or Model Predictive Controllers (MPC). Compared to the offline optimal control methods such as LQR, MPC exhibits more robustness to load fluctuations and parametric uncertainties in the grid model as it evaluates the control inputs based on the current state of the system at every time-step (Maciejowski, 2002). It also explicitly incorporates actuator constraints, which is important for WAC as the margin of variation for excitation voltages in supplementary controllers can be significantly limited (Kundur, 1994).

Several works in literature have proposed the use of a single MPC controller in the context of power systems. In Azad, Iravani, and Tate (2013), an MPC controller is proposed to modulate the reference point of a High Voltage Direct Current (HVDC) controller to damp inter-area oscillations. It is noted that HVDC can only be installed on a fixed transmission line, and hence might be less effective in damping oscillations originating from an electrically distant part of the grid. An adaptive version of centralized MPC is proposed in Ye and Liu (2013) which solves the problem of simultaneous control and identification of model parameters using subspace methods. Over recent years, MPC

* Corresponding author.
E-mail addresses: ajain18@ncsu.edu (A. Jain), achakra2@ncsu.edu (A. Chakrabortty), emrah.biyik@yasar.edu.tr (E. Biyik).

https://doi.org/10.1016/j.conengprac.2018.03.003
Received 24 August 2017; Received in revised form 24 February 2018; Accepted 2 March 2018

has also emerged as a popular choice for frequency regulation and load-frequency control (LFC). For example, in Ulbig, Arnold, Chatzivasileiadis, and Andersson (2011) cascaded MPCs are proposed to be deployed for multiple time-scale operations, so as to co-ordinate between the frequency control problem and the long-term power dispatch problem. This approach does not consider contingency scenarios such as faults on transmission lines, which can cause system instabilities. A constrained LFC problem is solved in Vazquez et al. (2014) with MPC, where the objective is to maintain high-frequency deviations in system frequency, caused due to load fluctuations, within acceptable limits. The effect of low-frequency oscillations is not considered. It is noted that all the above MPC methods applied to power systems are centralized methods, and hence do not consider the communication requirements for control.

Nomenclature

Section 2

i	Refers to the ith generator or the ith controller.
n, m	Number of power system states, and number of generators, respectively.
x, u, y	Vector of states, inputs and outputs, respectively.
δ, ω	Generator phase angle in radians and rotor velocity in per unit (p.u.), respectively.
$\acute{E}_q, \acute{E}_d$	q-axis and d-axis voltage behind transient reactances, respectively.
E_{fd}	Field excitation voltage in p.u.
V, I	Bus voltage and current, respectively, in p.u.
κ, M	Refers to the κ^{th} utility area and the number of utility areas, respectively.
$\mathfrak{c}, \mathfrak{p}$	Vector denoting PMU placement costs, and binary vector denoting absence/presence of PMUs.
$\mathcal{N}$	Number of buses in a given area.
$z, \tilde{z}$	Vector of generator algebraic variables, in polar and rectangular co-ordinates, respectively.
$\tilde{\chi}$	Vector of voltage and current measurements from PMU buses, in rectangular co-ordinates.
ϵ	Noise vector for PMU measurements with covariance matrix Σ.
T, k	Discrete-time sampling period and discrete time-step, respectively.

Section 3

$\mathbf{x}, \mathbf{u}, \mathbf{y}$	Vector of linearized states, control inputs and outputs, respectively.
A, B, C	State, control and output matrices for the linearized power system, respectively.
$\mathbf{x}_0$	Vector of post-disturbance linearized states.
$\mathcal{U}$	Linear constraint set for u.
λ, ρ	Eigenvalues and right eigenvectors of A, respectively.
$\bar{\rho}, \bar{\boldsymbol{\rho}}$	Eigenvalue (modal) residues and dominant modal residues, respectively.
$\mathcal{M}$	Modal matrix (matrix of eigenvectors) for A.
G	Represents a single generator node.

Section 4

N	DFT horizon as well as MPC prediction horizon.
$\bar{\mathcal{Y}}, \tilde{k}$	DFT vector with elements $\mathcal{Y}$, and frequency index, respectively.
W_N	DFT matrix with size $(N \times N)$.
Q	SDFT weighting matrix.
β^l, β^r	Left and right edges (in Hz) of the SDFT window, respectively.

Section 5

$\mathbb{P}(X)$	Power set of X, i.e. set of all subsets of X.
$\mathcal{A}$	Represents the set of modal areas $\{\mathcal{A}\}$.
C	Represents a single dMPC controller.
C^d, C^u	Set of downstream and upstream generators for C, respectively.
p, r	Number of modal areas and number of designed distributed controllers, respectively.
m_d, m_u	Number of generators in C^d and C^u, respectively.
$X \setminus Y$	Represents a set of elements which belong to set X but not to set Y.

Section 6

$\mathbf{z}, \mathbf{v}, \boldsymbol{\eta}$	Vectors for dMPC states, control inputs and outputs, respectively.
$\mathbf{w}$	Vector of communicated control inputs computed at the previous time-step.
T_z, T_v, T_w, T_η	Binary matrices for selection of $\mathbf{z}, \mathbf{v}, \mathbf{w}, \boldsymbol{\eta}$, respectively.
N_c	dMPC control horizon.
J	dMPC cost function to be minimized.
$\mathbb{Q}, \mathbb{R}, \mathbb{S}$	dMPC cost weighting matrices.
Δ	Operator for taking the difference between values at the current and previous time-steps.

Distributed MPC (dMPC), where multiple spatially distributed MPC controllers are used to satisfy a control objective, has also been proposed recently in literature for designing power system controllers. In various works (Camponogara, Jia, Krogh, & Talukdar, 2002; Franze & Tedesco, 2011; Mc Namara, Negenborn, De Schutter, & Lightbody, 2013; Mohamed, Bevrani, Hassan, & Hiyama, 2011; Negenborn, 2007; Venkat, Hiskens, Rawlings, & Wright, 2008), the LFC problem is solved in a distributed/decentralized manner using dMPC. Constraints are usually imposed on the output system frequency for tight regulation. However, these methods are not directly extendable to the WAC problem due to severe computational requirements for large-scale systems and inability to specifically target the inter-area oscillation modes. For instance, in Venkat et al. (2008) the authors propose multiple iterations for state-feedback communication within a single time-step, whereas in Mc Namara et al. (2013) a particle-swarm optimization method is proposed to reach a global solution with adaptive tuning of weights. Both these approaches will be prohibitive when applying these controllers to a WAC problem because of long communication delays and severe computational requirements. In contrast, the dMPC design proposed in this paper promotes communication sparsity for control while also successfully damping inter-area oscillations. A general review of dMPC designs can be found in Christofides, Scattolini, de la Pena, and Liu (2013).

To highlight the novelty of the proposed approach in this paper, it is noted that all of the above mentioned control schemes also suffer from either one or both of the following two additional drawbacks. First, they lead to a dense all-to-all communication topology between the generators amounting to a centralized implementation, and second, they are designed offline based on nominal models of the power system that are most often agnostic of where a disturbance may occur, or how this disturbance may impact the inter-area oscillations. In a recent paper (Jain, Chakrabortty, & Biyik, 2017) a sparse LQR controller was designed to counteract both of these drawbacks. In this paper that design is extended to a completely online MPC strategy that accommodates additional constraints on actuation. The oscillation damping problem is posed in terms of minimizing a quadratic objective function of the generator frequencies over a chosen time-horizon. A sparse state-feedback controller is developed to minimize this function following a disturbance in the grid with the sparsity pattern of the underlying communication

network being decided according to the modal residues of the inter-area oscillation modes excited by that disturbance. Generators that share high values of residues corresponding to a certain inter-area mode in open-loop are encouraged to communicate with each other for enhancing the damping of that mode in the closed-loop system. Note that these residues depend on the location and magnitude of the disturbance, and therefore can be different for different disturbance events. The choice of the sets of influential generators, and of the resulting communication topology in this design are, therefore, completely *aware* of the disturbance instead of being agnostic. The control signals are computed over this sparse topology using a distributed MPC design, and implemented as supplementary control inputs on top of existing PSS at selected sets of generators. The electromagnetic field excitation voltage of the generator is used as the actuation signal for the PSSs.

The rest of the paper is divided as follows. Section 2 provides a procedure for estimating the generator states required for the state-feedback controller. Section 3 identifies the set of generators which are the most influential in excitation of inter-area oscillation modes. The control objective is formed in Section 4 using Discrete Fourier Transforms (DFT) of predicted output trajectories. Next, the sparse communication topology is constructed in Section 5 based on the set of influential generators. Section 6 formulates the dMPC problem to be solved at every time-step based on the communication topology. Various simulation studies are shown in Section 7 to highlight the adaptability of the proposed controller to different disturbances, and Section 8 concludes the paper.

2. Power system state estimation

Consider a power system network with m synchronous generators. The network is assumed to be divided into M utility areas. All assets including generators, loads, PMUs, controllers, etc. in each area are owned and maintained by the utility company in charge of that area. Each company can choose to install multiple PMUs in its own area, but may or may not be willing to share its data with the other areas. Keeping in mind the above restrictions, an area-wise state estimation strategy is formulated in this section for feedback control of the generators.

Each generator is modeled by a fifth-order transient model, and is written in a compact form as:

$$\dot{x}_i(t) = g(x_i(t), z_i(t), u_i(t), a_i), \tag{1}$$

where $x_i = [\delta_i, \omega_i, \acute{E}_{qi}, \acute{E}_{di}, E_{fdi}]'$ are the generator states, $z_i = [|V_i|, \angle V_i, |I_i|, \angle I_i]'$ are the generator bus voltages and currents, and a_i is a vector of constant model parameters. The control input u_i is chosen as the stator field voltage E_{fdi}, and is constrained as $u_i^{min} \le u_i(t) \le u_i^{max}$ for all t, $\forall i = 1, \dots, m$. The reader is referred to (Sauer & Pai, 1997) for the exact expression of the nonlinear function $g(\cdot)$, as well as for the power flow equations relating the algebraic variables z_i to the states x_i.

The model (1) is a completely decentralized model since it is driven by variables belonging to the ith generator only. It is, however, not a state-space model as it contains the auxiliary variables z_i. The states x_i can be estimated for this model in a completely decentralized way if one has access to $z_i(t)$ at every instant of time. This can be assured by placing PMUs within each utility area such that the generator buses inside that area become geometrically observable, measuring the voltage and currents at the PMU buses, and thereafter computing z_i from those measurements. These steps are described next.

2.1. PMU placement for observability

In this section an area-wise optimal PMU placement (OPP) algorithm is provided, where the objective is to identify PMU bus locations (inside any utility area) such that the observability of generator buses is assured. This method differs from the classical OPP methods (Gomez-Exposito, Abur, Rousseaux, de la Villa Jaen, & Gomez-Quiles, 2011) since it does not require observability of all buses in the power network, thereby leading to a potentially lesser number of PMUs. The problem is formulated as follows.

For all utility areas $\kappa = 1, \dots, M$, the following integer programming problem is solved:

$$\min_{\mathfrak{p}_\kappa} \mathfrak{c}_\kappa' \mathfrak{p}_\kappa \tag{2a}$$

$$\text{s.t.} \quad Y_\kappa \mathfrak{p}_\kappa \ge \mathbb{1}_\kappa \ \text{ and } \ \mathfrak{p}_{\kappa,j} \in \{0, 1\}, \tag{2b}$$

where $\mathfrak{p}_{\kappa,j}$ denotes the jth element of $\mathfrak{p}_\kappa \in \mathbb{R}^{\mathcal{N}\times 1}$. Y_κ is the indicator matrix corresponding to the admittance matrix between buses in area κ; $\mathfrak{c}_\kappa \in \mathbb{R}^{\mathcal{N}\times 1}$ denotes the real-valued vector of relative costs for installing PMUs in area κ; and the elements of vector $\mathbb{1}_\kappa$ are given by:

$$\mathbb{1}_{\kappa,j} = \begin{cases} 1 & \text{if bus } j \text{ is a generator bus} \\ 0 & \text{otherwise.} \end{cases} \tag{3}$$

The solution of (2) will assure observability of all generator buses in the utility area κ, and also provide the optimal location of PMUs as the non-zero elements of the solution $\mathfrak{p}_\kappa^*$. It is noted that since this problem is non-convex, $\mathfrak{p}_\kappa^*$ is not unique but rather is one of the possible solutions with the minimum number of PMUs.

2.2. Generator state estimation

Next, using the noisy measurements from PMUs located at buses identified from solving (2), z_i for all generator buses inside the κ^{th} utility area are estimated, described as follows. Let z_κ denote the stacked vector $\{z_i\}$ for all i in the utility area κ. The linear measurement model is written as:

$$\tilde{\chi}_\kappa = H_\kappa \tilde{z}_\kappa + \epsilon_\kappa, \tag{4}$$

where $\tilde{z}_\kappa$ is the vector z_κ in rectangular co-ordinates, $\tilde{\chi}_\kappa$ is the vector of PMU measurements (voltages and currents on PMU buses in area κ) in rectangular co-ordinates, H_κ is a constant matrix of transmission line impedances, and ϵ_κ is the noise vector with covariance matrix Σ_κ (Zhou, Centeno, Thorp, & Phadke, 2006). A weighted least squares problem is the solved as:

$$\min_{\tilde{z}_\kappa} \Big[(\tilde{\chi}_\kappa - H_\kappa \tilde{z}_\kappa)' \Sigma_\kappa^{-1} (\tilde{\chi}_\kappa - H_\kappa \tilde{z}_\kappa) \Big]. \tag{5}$$

The solution is given by $\tilde{z}_\kappa^* = G_\kappa \tilde{\chi}_\kappa$, where $G_\kappa = (H_\kappa' \Sigma_\kappa^{-1} H_\kappa)^{-1} H_\kappa' \Sigma_\kappa^{-1}$ is the estimation gain. The voltages and currents in $\tilde{z}_\kappa^*$ are then converted back to polar co-ordinates. The procedure is done for every utility area κ, and at every time instant t, thereby providing the estimates $\hat{z}_i(t)$ for $z_i(t)$, $\forall i = 1, \dots, m$, in (1).

The continuous-time model (1) is sampled using forward Euler transformation to obtain a discrete-time model with sampling time $T = t/k$, where k is the discrete time-step. Using $\hat{z}_i(k)$ a Kalman filter is next designed to provide the ith generator state estimates:

$$\hat{x}_i(k+1) = \hat{x}_i(k) + T\bar{g}(\hat{x}_i(k), \hat{z}_i(k), u_i(k), a_i), \tag{6}$$

at any instant k. For details of this state estimator $\bar{g}(\cdot)$, which represents the model of an Unscented Kalman Filter (UKF), please see Singh & Pal (2014).

3. Post-disturbance modal participation

3.1. Linearized model

The variables $z_i(t)$ in (1) can be eliminated using the algebraic power flow equations for the network (skipped here for brevity) using a process called Kron reduction (Sauer & Pai, 1997). The resulting state-space model is linearized about the *loadflow* operating point (Kundur, 1994), and is discretized using the sampling time T. The resulting model, with $n = 5m$ number of total states, is written as:

$$\mathbf{x}(k+1) = A\mathbf{x}(k) + B\mathbf{u}(k), \text{ with } \mathbf{x}_0 \triangleq \mathbf{x}(0), \tag{7a}$$

$$\mathbf{y}(k) = \omega(k) - \omega_o = C\mathbf{x}(k), \text{ and } \mathbf{u}(k) \in \mathcal{U}^m, \tag{7b}$$

where $A \in \mathbb{R}^{n\times n}$, $B \in \mathbb{R}^{n\times m}$, $C = \text{blkdiag}(C_1, \dots, C_m) \in \mathbb{R}^{m\times n}$, ω_o is the rotor speed reference, and $\mathcal{U}^m = \mathcal{U}_1 \times \dots \times \mathcal{U}_m$ is the m-times cartesian product of the individual input constraint sets. The model is assumed to be excited by an exogenous but vanishing disturbance such as a fault, whose effect is captured by the post-disturbance 'initial' state $\mathbf{x}_0$. The fault signal considered in this paper is the three-phase fault in power grids, defined as either the current from overhead power lines flowing directly to earth (also called a line-to-ground fault), or a short-circuit among any of the three phase lines (also called a line-to-line fault). The linearized rotor speeds are chosen as the performance variables $\mathbf{y}(k) = [y_1(k), \dots, y_m(k)]'$, which describe the kinetic energy of the system. Other electromechanical variables, such as paired difference of phase angles between generators describing the potential energy of the system can also be used in the design objective, if needed. It is assumed that A is bounded-input bounded-output stable, and (A, B) is stabilizable.

3.2. Open-loop modal analysis

The goal is to enhance the damping of the low-frequency oscillations of (7) in closed-loop. This objective is formulated using an online predictive approach in terms of minimizing a quadratic energy function of $y_i(k)$, $\forall i = 1, \dots, m$, formulated in Section 4. Next, it is shown how a central coordinator (CCO), such as an Independent Systems Operator, using $\hat{\mathbf{x}}_0$ estimated by various UKFs, estimates the modal residues of $y_i(k)$, from which it can decide the sparsity structure of the wide-area communication network.

From linear system theory, the system outputs can be written in the modal decomposition form:

$$y_i(k) = C_i \sum_{j=1}^{n} \alpha_j \rho_j \lambda_j^k = \sum_{j=1}^{n} \bar{\rho}_{ij} \lambda_j^k, \tag{8}$$

where the eigenvalues $\{\lambda_j\}$ are assumed to be distinct. $\{\alpha_i\}$ are scalars, given by $\boldsymbol{\alpha} = \mathcal{M}^{-1}\hat{\mathbf{x}}_0$ where $\boldsymbol{\alpha} = [\alpha_1, \dots, \alpha_n]'$, and $\mathcal{M} = \text{col}(\rho_1, \dots, \rho_n)$. Hence, it is clear that once the CCO knows $\hat{\mathbf{x}}_0$ (which depends on the magnitude and location of the unknown exogenous disturbance), it can estimate $\hat{\boldsymbol{\alpha}}$, and therefore, the modal residues $\{\bar{\rho}_{ij}\}$. Note that the implicit assumption here is that the CCO has full knowledge of the matrix A. For damping control, the proposed design will be focused only on the inter-area modes (i.e. oscillation modes with signal frequencies between 0.1 and 2 Hz). However, *dominance* of these modes is defined not based on their frequencies, but on their output residues. For example, consider a power system with five generators, with each generator considered as a coherent area in itself yielding 4 inter-area modes. The impulse response of the small-signal frequencies of the five generators can be written as:

$$\begin{aligned}
G_1 &: y_1(k) = \bar{\rho}_{11}\lambda_1^k + \bar{\rho}_{12}\lambda_2^k + \bar{\rho}_{13}\lambda_3^k + \bar{\rho}_{14}\lambda_4^k + b_1(k),\\
G_2 &: y_2(k) = \bar{\rho}_{21}\lambda_1^k + \bar{\rho}_{22}\lambda_2^k + \bar{\rho}_{23}\lambda_3^k + \bar{\rho}_{24}\lambda_4^k + b_2(k),\\
G_3 &: y_3(k) = \bar{\rho}_{31}\lambda_1^k + \bar{\rho}_{32}\lambda_2^k + \bar{\rho}_{33}\lambda_3^k + \bar{\rho}_{34}\lambda_4^k + b_3(k),\\
G_4 &: y_4(k) = \bar{\rho}_{41}\lambda_1^k + \bar{\rho}_{42}\lambda_2^k + \bar{\rho}_{43}\lambda_3^k + \bar{\rho}_{44}\lambda_4^k + b_4(k),\\
G_5 &: y_5(k) = \bar{\rho}_{51}\lambda_1^k + \bar{\rho}_{52}\lambda_2^k + \bar{\rho}_{53}\lambda_3^k + \bar{\rho}_{54}\lambda_4^k + b_5(k),
\end{aligned} \tag{9}$$

where $b_i(k) = \sum_{j=1}^{4} \bar{\rho}_{ij}^* \lambda_j^{*k} + y_i^f(k)$ with $(^*)$ denoting complex conjugation; and $y_i^f(k)$ is the high-frequency modal component. Let the residues $\bar{\boldsymbol{\rho}}_{11}$, $\bar{\boldsymbol{\rho}}_{21}$, $\bar{\boldsymbol{\rho}}_{22}$, $\bar{\boldsymbol{\rho}}_{32}$, and $\bar{\boldsymbol{\rho}}_{51}$, marked in boldface, be termed as *dominant* residues. Dominance is defined such that all $|\bar{\rho}_{ij}| \geq \mu$, where μ is a pre-specified threshold. This threshold can be chosen by the CCO in different ways, one possible choice being the arithmetic mean of all residues:

$$\mu \triangleq \frac{1}{m(m-1)} \sum_{i=1}^{m} \sum_{j=1}^{m-1} |\bar{\rho}_{ij}|. \tag{10}$$

In other words, it is assumed that only the inter-area modes λ_1, λ_2 are substantially excited by the incoming disturbance while the other inter-area modes have poorer participation in the rotor speed responses. Similar assumptions on excitation of selective modes has been done in literature such as in Pérez-Arriaga, Verghese, and Schweppe (1982). The residue magnitudes are then collected in a so-called modal participation (MP) matrix that shows which generators contribute most to the excitation of which dominant mode. For this example, generators G_1, G_2, G_5 contribute significantly to mode λ_1, and generators G_2, G_3 to mode λ_2. Information about this grouping is used to decide the topology of communication. Detailed description of this will be given in Section 5.

Note that two different disturbance events can result in two significantly different $\hat{\mathbf{x}}_0$, and hence, two significantly different MP matrices (see Fig. 4(a)–(c) for an example), indicating different sets of generators influencing different combinations of the inter-area modes. It is important for a controller to be aware of this dominance property instead of an offline controller that is agnostic to it. This is why the proposed controller is designed in real-time after the fault.

4. Control objective

Next, the control objective is formulated by deriving a cost function that reflects all the *dominant* modes identified by the CCO using the method described in Section 3.2. The concept of SDFT is introduced for damping of selected modes in a power system. Let the output trajectory of the ith generator, starting at time-step k, be $\bar{y}_i(k) = [y_i(k), y_i(k+1), \dots, y_i(k+N-1)]'$. The N-point DFT of $\bar{y}_i$, $\forall i = 1, \dots, m$, at time-step k can be written as:

$$\mathcal{Y}_i(\tilde{k}|k) = \sum_{k=0}^{N-1} y_i(k) e^{-\jmath 2\pi \tilde{k} k/N}, \quad \forall \tilde{k} = 0, \dots, N-1, \tag{11}$$

where $\tilde{k}$ is the DFT frequency index. The above expression can be written in a matrix form as:

$$\bar{\mathcal{Y}}_i[0 : N-1|k] = W_N \bar{y}_i(k), \tag{12}$$

where $\bar{\mathcal{Y}}_i[0 : N-1|k] = [\mathcal{Y}_i(0|k), \dots, \mathcal{Y}_i(N-1|k)]'$, and $W_N \in \mathbb{C}^{N\times N}$ is the N-point complex DFT matrix:

$$W_N = \frac{1}{\sqrt{N}} \begin{bmatrix} 1 & 1 & \cdots & 1 \\ 1 & w & \cdots & w^{(N-1)} \\ 1 & w^2 & \ddots & w^{2(N-1)} \\ \vdots & & & \vdots \\ 1 & w^{(N-1)} & \cdots & w^{(N-1)(N-1)} \end{bmatrix}, \tag{13}$$

with $w \triangleq e^{-\jmath\frac{2\pi}{N}}$ being the complex exponential. Here, $\mathcal{Y}_i(0|k)$ is the DC component, $[\mathcal{Y}_i(1|k), \dots, \mathcal{Y}_i(N/2|k)]$ are the positive frequency components, and $[\mathcal{Y}_i(N/2+1|k), \dots, \mathcal{Y}_i(N-1|k)]$ are the negative frequency components. Since $\bar{y}_i(k)$ is real-valued, the magnitudes of the positive and negative frequency components are equal in the DFT spectrum. In order to extract a selected range of positive frequency components from (12), the appropriate rows of W_N can be chosen to define the N-point SDFT as:

$$\bar{\mathcal{Y}}_i[\beta_i^l : \beta_i^r|k] = W_{i,N} \bar{y}_i(k), \tag{14}$$

where $[\beta_i^l, \beta_i^r]$ is the desired frequency window, and $W_{i,N} \in \mathbb{C}^{(\beta_i^r - \beta_i^l)\times N}$ is a submatrix of (13) containing the corresponding rows. β_i^l, β_i^r represent the left and right window edges respectively. For us the choice of the center of this window is the frequency of any dominant mode, whereas β_i^l, β_i^r are chosen such that the width is proportional to the steepness of the peaks of (11). From (14), the modal cost to be minimized is written as:

$$\mathcal{E}_i(k) = \sum_{\tilde{k}=\beta_i^l}^{\beta_i^r} |\mathcal{Y}(\tilde{k}|k)|^2 = 2\bar{y}_i(k)'\hat{Q}_i\bar{y}_i(k), \tag{15}$$

with the SDFT output weighting matrix:

$$Q_i = (W_{i,N}^{real})'(W_{i,N}^{real}) + (W_{i,N}^{imag})'(W_{i,N}^{imag}). \tag{16}$$

The matrices $W_{i,N}^{real}$, $W_{i,N}^{imag}$ contain the real and imaginary parts of $W_{i,N}$ respectively. It is easy to show that for $\beta_i^l = 0$ and $\beta_i^r = N-1$, i.e. if

the selected window encompasses the full frequency spectrum, then Q_i becomes an identity matrix, and therefore (15) becomes the usual quadratic energy of the outputs with unity weighting.

Remark 1. Note that the choice for the center of SDFT window is based on the frequencies of the open-loop eigenvalues of A. Minimizing (15), however, would require an estimate of frequencies of the dominant eigenvalues of the closed-loop model. Hence, an implicit assumption behind the cost (15) is that the applied control does not alter the frequency of closed-loop modes from their open-loop values to a significant extent. This assumption has been used in previous literature such as in Larsen et al. (1995), and is verified with simulation results in Section 7. If, however, the frequencies of the inter-area modes change from open- to closed-loop, the width of SDFT window can accommodate this shift.

5. Communication architecture for control

The controller communication architecture is developed next, based on the choice of influential generators for the dominant modes.

5.1. Notation

For an arbitrary set $\boldsymbol{X}$, its individual elements are denoted by X_i. A *power set* $\mathbb{P}(\boldsymbol{X})$ is defined as the set of all its subsets, e.g. for $\boldsymbol{X} = \{X_1, X_2\}$, the power set is the *collection* (set of sets) $\mathbb{P}(\boldsymbol{X}) = \{X_1, X_2, \{X_1, X_2\}, \emptyset\}$. A mapping $h : \mathbb{P}(\boldsymbol{X}) \mapsto \bar{P}(\boldsymbol{X})$ is defined such that:

$$\bar{P}_i = \begin{cases} \bigcap_j \mathbb{P}_{i,j} & \text{if } \mathbb{P}_i \text{ is a collection,} \\ \mathbb{P}_i & \text{if } \mathbb{P}_i \text{ is not a collection,} \end{cases} \tag{17}$$

where $\mathbb{P}_{i,j}$ is the jth element of the collection $\mathbb{P}_i$. Hence, after applying h, no element of $\bar{P}(\boldsymbol{X})$ is a collection. Also, let $P(\boldsymbol{X}) \triangleq \bar{P}(\boldsymbol{X}) \setminus \emptyset$. Additional mappings g_1, g_2 are defined, where g_1 maps intersecting elements to symbolic forms as $g_1(\{X_1 \cap X_2, X_3 \cap X_4\}) = \{X_{12}, X_{34}\}$, and g_2 maps any symbolic form to its set unions, i.e. $g_2(\{X_{12}, X_{34}\}) = \{X_1 \cup X_2, X_3 \cup X_4\}$. The domain of h is the set of generators $\{G_1, \dots, G_m\}$, and the range of h is given by (17).

5.2. Sparse communication architecture

Let the set of generators that exhibit the greatest influence on the excitation of the jth dominant mode be denoted as $\mathcal{A}_j$, referred to as the jth *modal area*. For the 5-machine example in Section 3.2, the dominant modes are λ_1, λ_2, and the corresponding modal areas are $\mathcal{A}_1 = \{G_1, G_2, G_5\}$, $\mathcal{A}_2 = \{G_2, G_3\}$. Two or more modal areas can be overlapping iff any mode in the set of dominant modes are influenced by more than one generator. This is the case for generator G_2 in the example.

The proposed distributed control strategy then involves designing r number of controllers, where r is the sum of p number of dominant modes, and the number of overlappings between modal areas, if any. Hence, a single dedicated controller is assigned to each modal area, where its objective is to minimize the modal cost (15). The underlying communication infrastructure is defined by:

- *Upstream links*: these links originate from the controller, and transmit control signals to its assigned generators, and
- *Downstream links*: these links originate from the generators, and transmit their states to their respective controllers.

Additionally, controllers may talk to a specific subset of other controllers, where this subset is decided by the overlapping modal areas. The intuition behind this communication strategy is that in order to design a controller C_i, $\forall i = 1, \dots, r$, that minimizes a modal cost corresponding to oscillation mode λ_i, only those set of generators are important that show dominant participation in λ_i in their predicted output response.

The architecture can then be formalized as follows. Let the set of all identified p modal areas be: $\boldsymbol{\mathcal{A}} = \{\mathcal{A}_1, \dots, \mathcal{A}_p\}$. Since the modal areas can be overlapping, the non-empty intersecting subsets of $\boldsymbol{\mathcal{A}}$ are denoted by $P(\boldsymbol{\mathcal{A}}) = h(\mathbb{P}(\boldsymbol{\mathcal{A}})) \setminus \emptyset$. Let $P(\boldsymbol{\mathcal{A}}) = P^d(\boldsymbol{\mathcal{A}}) \cup P^o(\boldsymbol{\mathcal{A}})$, where $P^d(\boldsymbol{\mathcal{A}})$ contains the sets for dominant modal areas, and $P^o(\boldsymbol{\mathcal{A}})$ contains the intersecting sets for overlapping modal areas. Then the set of generators which receive their control inputs from controller C_i, $\forall i = 1, \dots, r$, connected via the upstream links, is given by:

$$C_i^u = \begin{cases} \{G_l \in P_i \mid G_l \notin P_j\} & \text{if } P_i \in P^d(\boldsymbol{\mathcal{A}}) \\ \{G_l \in P_i \mid g_1(P_i) \notin g_1(P_j)\} & \text{if } P_i \in P^o(\boldsymbol{\mathcal{A}}), \end{cases} \tag{18}$$

for all $j = \{1, \dots, p\}$, $j \neq i$ with generator index $l \in \{1, \dots, m\}$, and $m_{u,i} = \text{card}(C_i^u)$. (18) conveys assigning controllers to generators such that each controller is minimizing a unique modal cost specific to the generator's modal area. Finally, the set of generators is constructed for downstream communication to each controller C_i as:

$$C_i^d = \begin{cases} \{G_l \in P_i\} & \text{if } P_i \in P^d(\boldsymbol{\mathcal{A}}) \\ \{G_l \in g_2(g_1(P_i))\} & \text{if } P_i \in P^o(\boldsymbol{\mathcal{A}}), \end{cases} \tag{19}$$

where $m_{d,i} = \text{card}(C_i^d)$. (19) conveys assigning generators to the controller C_i from where state feedback is needed.

The steps for constructing this communication architecture over time are illustrated in Fig. 1 using the 5-machine example in (9). The physical states of the generators $G_1 - G_5$ are coupled with each other via Kron reduction, and hence the leftmost figure shows all five generators to be connected to each other. Starting from time-step $k = 0$ (fault-clearing), the CCO uses a small number of time-steps, say k^*, to compute the MP matrix, and determine that in this case the system needs to be divided into two modal areas $\mathcal{A}_1, \mathcal{A}_2$ with dominant frequency modes λ_1, λ_2, respectively, where $\mathcal{A}_1 = \{G_1, G_2, G_5\}$ and $\mathcal{A}_2 = \{G_2, G_3\}$. The power set is $\mathbb{P}(\boldsymbol{\mathcal{A}}) = \{\mathcal{A}_1, \mathcal{A}_2, \{\mathcal{A}_1, \mathcal{A}_2\}, \emptyset\}$, and $h(\mathbb{P}(\boldsymbol{\mathcal{A}})) \setminus \emptyset = P(\boldsymbol{\mathcal{A}}) = \{\mathcal{A}_1, \mathcal{A}_2, \mathcal{A}_1 \cap \mathcal{A}_2\} = \{\mathcal{A}_1, \mathcal{A}_2\} \cup \{\mathcal{A}_1 \cap \mathcal{A}_2\} \triangleq P^d(\boldsymbol{\mathcal{A}}) \cup P^o(\boldsymbol{\mathcal{A}})$. As shown, three controllers are then designed with respective sets of upstream and downstream links defined by the sets:

$$C_1^u = \{G_l \in P_1 \mid G_l \notin P_2, P_3\} = \{G_1, G_5\} \tag{20a}$$
$$C_2^u = \{G_l \in P_2 \mid G_l \notin P_1, P_3\} = \{G_3\} \tag{20b}$$
$$C_3^u = \{G_l \in P_3 \mid g_1(P_3) \notin \mathcal{A}_1, \mathcal{A}_2\} = \{G_2\} \tag{20c}$$
$$C_1^d = \{G_l \in P_1\} = \{G_1, G_2, G_5\} \tag{20d}$$
$$C_2^d = \{G_l \in P_2\} = \{G_2, G_3\} \tag{20e}$$
$$C_3^d = \{G_l \in g_2(g_1(P_3))\} = \{G_1, G_2, G_3, G_5\}, \tag{20f}$$

where $g_1(P_3) = g_1(\mathcal{A}_1 \cap \mathcal{A}_2) = \mathcal{A}_{12}$, and $g_2(g_1(P_3)) = \mathcal{A}_1 \cup \mathcal{A}_2$. Sets (20a), (20b), (20d), (20e) correspond to the condition $P_i \in P^d(\boldsymbol{\mathcal{A}})$ being true, and the sets (20c),(20f) correspond to the condition $P_i \in P^o(\boldsymbol{\mathcal{A}})$ being true. These links can be seen in Fig. 1 for the three controllers $C_1 - C_3$. The presence of a third controller is due to the overlap between the modal areas, resulting in controller-to-controller links denoted by $\mathbf{U}_{1,3}$ and $\mathbf{U}_{2,3}$. It is noted that the system shown in Fig. 1 is a simple example used for illustrative purposes. For power systems with much larger size, the savings in communication from the proposed distributed controller over a centralized controller will be significant, as will be shown in Section 7.

5.3. Cyber–physical architecture

It is noted that since the indices of generators associated with any controller C_i are not fixed *a-priori* due to the unpredictable nature of disturbances, it is not advisable to install C_i at any fixed generator site, but rather in a shared computational platform such as a cloud network (Annaswamy, Hussain, Chakrabortty, & Cvetkovic, 2016). Controller implementation is explained in the following.

Each utility area is assumed to have a Phasor Data Concentrator (PDC). Each PDC is assumed to have access to a local cloud at its local

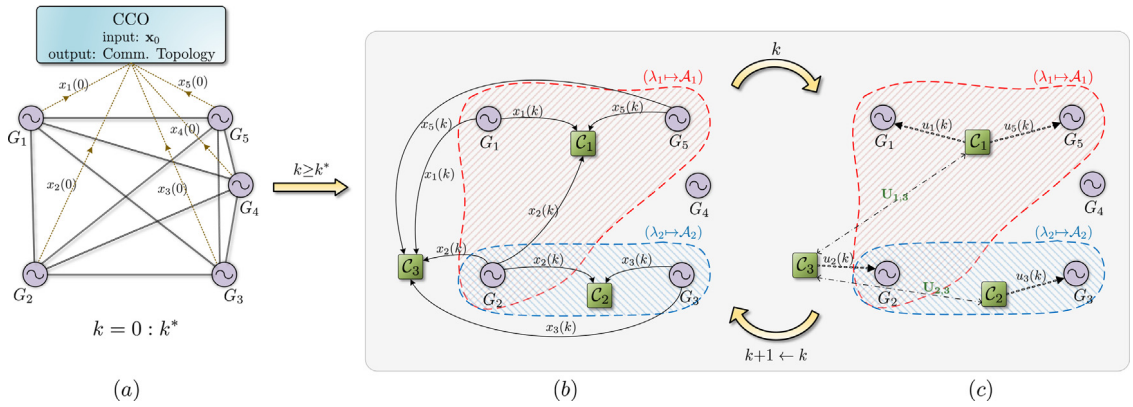

Fig. 1. Architecture of the proposed distributed control system, shown on a five-generator power system example, following (9). Subfigure (a) shows the physical interconnections between generators in the Kron-reduced form. CCO receives $\hat{\mathbf{x}}_0$ from all generators and using the MP matrix decides the communication architecture, within the time-steps $k = 0 : k^*$. CCO then informs all generators about the communication topology. Subfigures (b) and (c) show state and control communications respectively for $k \geq k^*$, with the three dMPC controllers in feedback. The two identified modal areas are highlighted in red and blue. (For interpretation of the references to color in this figure legend, the reader is referred to the web version of this article.)

control center, which is part of a larger cloud network referred to as the *Internet of Clouds*. PMUs in the utility area κ measure the phasor voltages and currents at designated buses, and transmit them to their local PDC. The PDC in area κ then transmits this information to the local cloud. State estimation for all generators in this utility area is done with an estimator E_κ using (4)–(6) in the local cloud.

This process goes on round the clock. Suppose at $k = 0$ a fault occurs in the system. The state vector $\hat{\mathbf{x}}_\kappa(0)$ is communicated from the local clouds to the CCO. The CCO, after receiving the entire state vector $\hat{\mathbf{x}}_0 = [\hat{\mathbf{x}}_1(0), \dots, \hat{\mathbf{x}}_\kappa(0), \dots, \hat{\mathbf{x}}_M(0)]'$, decides the communication topology following the steps outlined in Section 5.2. The CCO then informs the controller assignments to the local clouds, where controllers C_i, $\forall i = 1, \dots, r$, are created. At every time-step, after receiving the estimated states according to the set C_i^d, these controllers then solve the dMPC optimization problem (to be described in Section 6). Finally, the local clouds communicate the computed control inputs to generator actuators according to the set C_i^u. The communication network between the PDCs and the local clouds is a Local Area Network (LAN), while the network between different clouds in the *Internet of Clouds* is a Wide Area Network (WAN). Please see Algorithm 1 for step-by-step description of this implementation.

The above procedure is illustrated with the 5-machine example (9), as shown in Fig. 2. For simplicity, it is assumed that each of the five machines belong to a distinct utility area. Since G_4 is not contained in any of the modal areas, only four clouds (corresponding to utility areas 1, 2, 3 and 5) are shown. To minimize communication inside the internet of clouds, C_1 is placed in the local cloud for utility area 1, C_3 in the local cloud for utility area 2, and C_2 in the local cloud for utility area 3. Cloud-to-cloud links I_{ij}, where i, j are the indices for sending and receiving clouds respectively, are set up for the controllers to exchange necessary information. Their information content is given in the caption of Fig. 2. In this figure the previous time-step control trajectory for the ith generator is denoted by $\bar{u}_i(k-1) \triangleq [u_i(k|k-1), \dots, u_i(k+N_c-1|k-1)]'$.

6. Distributed MPC

Using the communication architecture defined above, a distributed MPC control problem is formulated next.

6.1. Distributed controller prediction modeling

To select a subset of states, outputs and control inputs, let $\mathbf{z}_i = T_{\mathbf{z}_i}\mathbf{x}$, $\mathbf{v}_i = T_{\mathbf{v}_i}\mathbf{u}$, $\mathbf{w}_i = T_{\mathbf{w}_i}\mathbf{u}$, $\boldsymbol{\eta}_i = T_{\boldsymbol{\eta}_i}\mathbf{y}$, where $T_{\mathbf{z}_i} \in \mathbb{R}^{n_{d,i} \times n}$, $T_{\mathbf{v}_i} \in \mathbb{R}^{m_{u,i} \times m}$, $T_{\mathbf{w}_i} \in \mathbb{R}^{(m_{d,i} - m_{u,i}) \times m}$ and $T_{\boldsymbol{\eta}_i} \in \mathbb{R}^{m_{u,i} \times 1}$ are indicator matrices whose structures follow from the communication architecture for controller C_i; $n_{d,i}$ represents the total number of states for the generators associated with the downstream links set C_i^d; $\mathbf{z}_i$ is the vector of states belonging to generators associated only with the downstream links; $\mathbf{v}_i$ is the vector of optimized control inputs to actuators only associated with the upstream links; $\boldsymbol{\eta}_i$ is the vector of outputs from generators only associated with the downstream links; $\mathbf{w}_i$ is the vector of communicated control inputs computed at the previous time-step by other controllers, and communicated to C_i. The model for the set of generators associated with C_i, $\forall i = 1, \dots, r$, can then be written as:

$$\mathbf{z}_i(k+1) = A_{\mathbf{z}_i}\mathbf{z}_i(k) + B_{\mathbf{v}_i}\mathbf{v}_i(k) + B_{\mathbf{w}_i}\mathbf{w}_i(k), \tag{21a}$$

$$\boldsymbol{\eta}_i(k) = C_{\boldsymbol{\eta}_i}\mathbf{z}_i(k), \tag{21b}$$

where $A_{\mathbf{z}_i} = T_{\mathbf{z}_i} A T'_{\mathbf{z}_i}$, $B_{\mathbf{v}_i} = T_{\mathbf{z}_i} B T'_{\mathbf{v}_i}$, $B_{\mathbf{w}_i} = T_{\mathbf{z}_i} B T'_{\mathbf{w}_i}$ and $C_{\boldsymbol{\eta}_i} = T_{\mathbf{z}_i} C T'_{\boldsymbol{\eta}_i}$. Outputs $\boldsymbol{\eta}_i(k)$ thus represent an approximation to the actual generator outputs. Moving (21b) forward in time, the output prediction trajectory with horizon N and control horizon N_c (with $N \geq N_c$) can be written as:

$$\bar{\boldsymbol{\eta}}_i(k) = \Lambda_i \mathbf{z}_i(k) + \Phi_{\mathbf{v}_i}\bar{\mathbf{v}}_i(k) + \Phi_{\mathbf{w}_i}\bar{\mathbf{w}}_i(k), \tag{22}$$

where $\bar{\boldsymbol{\eta}}_i, \bar{\mathbf{v}}_i, \bar{\mathbf{w}}_i$ denote the trajectories:

$$\bar{\boldsymbol{\eta}}_i(k) = [\boldsymbol{\eta}_i(k|k)', \dots, \boldsymbol{\eta}_i(k+N-1|k)']', \tag{23a}$$

$$\bar{\mathbf{v}}_i(k) = [\mathbf{v}_i(k|k)', \dots, \mathbf{v}_i(k+N_c-2|k)']', \tag{23b}$$

$$\bar{\mathbf{w}}_i(k) = [\mathbf{w}_i(k|k)', \dots, \mathbf{w}_i(k+N_c-2|k)']', \tag{23c}$$

and $\Lambda_i, \Phi_{\mathbf{v}_i}, \Phi_{\mathbf{w}_i}$ are block matrices easily constructed from $A_{\mathbf{z}_i}, B_{\mathbf{v}_i}, B_{\mathbf{w}_i}$, $C_{\boldsymbol{\eta}_i}$. It is noted that due to the distributed nature of the communication architecture, the controller C_i does not have access to $\bar{\mathbf{w}}_i(k)$. Hence, for this control design $\bar{\mathbf{w}}_i(k)$ is considered to be the control trajectory computed at the previous time-step by another controller C_j, and make sure that C_i, C_j communicate so that C_i can utilize this trajectory for its local predictions. For this reason the difference between the optimized control trajectory at the current and previous time-steps is penalized in (24). Also, because the states are not directly measurable, C_i will only receive $\hat{\mathbf{z}}_i(k)$ for feedback instead of $\mathbf{z}_i(k)$. In the subsequent sections the notations for the variables defined in (23) are used, but it is assumed that the RHS follows from $\hat{\mathbf{z}}_i(k)$ instead of $\mathbf{z}_i(k)$.

6.2. dMPC with modal cost

The objective of each dMPC controller C_i is to minimize the energy content of the SDFT spectrum of the generators assigned to it, while also respecting both actuation and communication constraints. For a

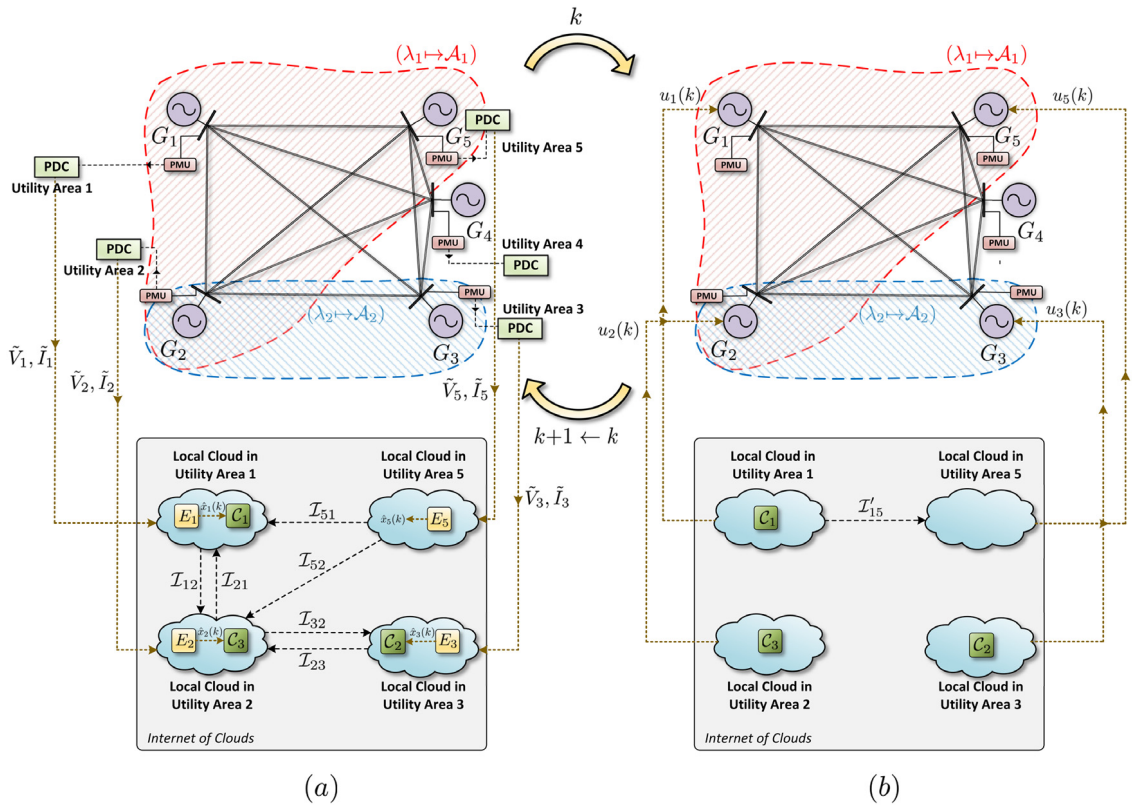

Fig. 2. Cyber–Physical Architecture for dMPC, shown on the five-generator example, following (9). For this example, since it is assumed that each generator bus has a PMU installed, the output of the ith PDC will be the generator bus voltage V_i, and the line currents I_i measured on all transmission lines connected to the generator bus. The cloud-to-cloud communication links are given as: $\mathcal{I}_{21}(k) = \mathcal{I}_{32}(k) = \{\hat{x}_2(k), \bar{u}_2(k-1)\}$, $\mathcal{I}_{51}(k) = \{\hat{x}_5(k)\}$, $\mathcal{I}_{12}(k) = \{\hat{x}_1(k), \bar{u}_1(k-1)\}$, $\mathcal{I}_{52}(k) = \{\hat{x}_5(k), \bar{u}_5(k-1)\}$, $\mathcal{I}_{23}(k) = \{\hat{x}_3(k), \bar{u}_3(k-1)\}$ and $\mathcal{I}'_{15}(k) = \{u_5(k)\}$.

controller C_i, $\forall i = 1, \ldots, r$, a cost function using the feedback $\hat{\mathbf{z}}_i(k)$ is formulated as:

$$J_i(\hat{\mathbf{z}}_i(k)) = \bar{\boldsymbol{\eta}}_i(k)' \mathbb{Q}_i \bar{\boldsymbol{\eta}}_i(k) + \bar{\mathbf{v}}_i(k)' \mathbb{R}_i \bar{\mathbf{v}}_i(k) + \Delta\bar{\mathbf{v}}_i(k)' \mathbb{S}_i \Delta\bar{\mathbf{v}}_i(k), \tag{24}$$

where $\Delta\bar{\mathbf{v}}_i(k) = \bar{\mathbf{v}}_i(k) - \bar{\mathbf{v}}_i(k-1)$ is the difference between the current and previous time-step optimized control trajectories; $\mathbb{R}_i$ and $\mathbb{S}_i$ are positive definite weighting matrices of size $m_{u,i}(N_c - 1)$; and $\mathbb{Q}_i$ is a semi-positive definite block diagonal output trajectory weighting matrix of size $m_{u,i}N$ such that $\mathbb{Q}_i = \text{blkdiag}(Q_i, \ldots, Q_i)$ with Q_i as the SDFT matrix constructed for frequency weighting in (16). The dMPC problem for the ith controller is given by:

$$\mathcal{P}_i : \quad \min_{\bar{\mathbf{v}}_i(k)} \; J_i(\hat{\mathbf{z}}_i(k)) \tag{25a}$$

$$\text{s.t.} \;\; \mathbf{v}_i(t) \in \mathcal{U}^{m_{u,i}}, \;\; \forall t \in [k, \ldots, k + N_c - 1], \tag{25b}$$

$$\mathbf{w}_i(t) = T_{w_i} \mathbf{u}(t|k-1), \;\; \forall t \in [k, \ldots, k + N_c - 1], \tag{25c}$$

where $\mathcal{U}^{m_{u,i}}$ is the control input constraint set. From (24), $\mathbb{Q}_i \geq 0$ and $\mathbb{R}_i, \mathbb{S}_i > 0$, hence the cost J_i is convex. $\mathcal{P}_i$ in the standard *Quadratic Programming* form is given by:

$$J_i(\hat{\mathbf{z}}_i(k)) = \frac{1}{2} \bar{\mathbf{v}}_i(k)' \boldsymbol{\mathcal{H}}_i \bar{\mathbf{v}}_i(k) + \boldsymbol{c}_i(k)' \bar{\mathbf{v}}_i(k) + \epsilon_i, \tag{26}$$

where $\boldsymbol{\mathcal{H}}_i = 2(\boldsymbol{\Phi}'_{v_i} \mathbb{Q}_i \boldsymbol{\Phi}_{v_i} + \mathbb{R}_i + \mathbb{S}_i)$ and $\boldsymbol{c}_i(k)' = 2[\mathbf{z}_i(k) \Lambda'_i \mathbb{Q}_i \boldsymbol{\Phi}_{v_i} + \bar{\mathbf{w}}(k)' \boldsymbol{\Phi}'_{w_i} \mathbb{Q}_i \boldsymbol{\Phi}_{v_i} - \bar{\mathbf{v}}_i(k-1)' \mathbb{S}_i]$. The terms collected in the scalar ϵ_i are ignored while solving $\mathcal{P}_i$ since they do not contain the optimization variable $\bar{\mathbf{v}}_i(k)$.

Remark 2. The horizon length (equal to the SDFT length) N is a design parameter that should be tuned considering the following trade-off. Since the cost (24) is the energy content of a specific frequency window, the SDFT length N should be long enough to get an adequate frequency resolution $1/(TN)$ for selecting the SDFT window. On the other hand, a very large value of N can result in large prediction errors.

6.3. Closed-loop stability

This section provides *a-posteriori* sufficient conditions for dMPC closed-loop stability of the system. Substituting (22) in (24):

$$J_i(\hat{\mathbf{z}}_i(k)) = \hat{\mathbf{z}}'_i(k)(\Lambda'_i \mathbb{Q}_i \Lambda_i)\hat{\mathbf{z}}_i(k) + F_i(\hat{\mathbf{z}}_i(k)), \tag{27}$$

where, for the simplified case of a single-step control horizon, $F_i(\hat{\mathbf{z}}_i(k))$ is quadratic in $\mathbf{v}_i(k), \mathbf{w}_i(k), \Delta\mathbf{v}_i(k)$, and linear in $\hat{\mathbf{z}}_i(k)$. Substituting (21) in (27) at time $k+1$, and then subtracting (27):

$$J_i(\hat{\mathbf{z}}_i(k+1)) - J_i(\hat{\mathbf{z}}_i(k)) = \hat{\mathbf{z}}'_i(k) M_i \hat{\mathbf{z}}_i(k) + G_i(\hat{\mathbf{z}}_i(k)), \tag{28}$$

where $M_i = A'_{z_i} \Lambda'_i \mathbb{Q}_i \Lambda_i A_{z_i} - \Lambda' \mathbb{Q}_i \Lambda_i$, and $G_i(\hat{\mathbf{z}}_i(k)) = F_i(\hat{\mathbf{z}}_i(k+1)) - F_i(\hat{\mathbf{z}}_i(k))$. Next, the following result is provided for closed-loop stability (Alessio & Bemporad, 2007 Theorem 2).

Theorem 1 (*Alessio & Bemporad, 2007*). *Considering the matrix M_i and the scalar-valued function $G_i(\cdot)$ in (28), $\forall i = 1, \ldots, r$, if the following condition:*

$$\mathbf{x}' \Big(\sum_{i=1}^{r} T'_{z_i} M_i T_{z_i} \Big) \mathbf{x} + \sum_{i=1}^{r} G_i(T_{z_i} \mathbf{x}) < 0 \tag{29}$$

is satisfied $\forall \mathbf{x} \in \mathbb{R}^n$, then (7) is closed-loop stable under dMPC.

It is clear from (29) that closed-loop stability of (7) will explicitly depend on the sparsity of the communication network. If for a given level of sparsity the test (29) fails, then the threshold μ in (10) can be

Algorithm 1 Algorithm for Implementing Proposed dMPC Controller

1: Location of PMUs is determined by solving the OPP problem (2) described in Section 2.1. This is a planning problem, and can be solved offline by the system operator. PMUs are then installed at these locations.
2: At all times (before, during, after a fault), each local PDC continuously collects voltage and current measurements from all PMUs in area κ, and sends this data to its local cloud as shown in Fig. 2.
3: In each local cloud, this measurement data is fed to a local estimator E_κ which first estimates the phasors for all generator buses by solving (5), and then estimates the generator states $\mathbf{x}_\kappa$ using the Kalman filter (6), for all generators in area κ. These states $\hat{\mathbf{x}}_\kappa$ are used for the continuous monitoring of area dynamics.
4: At steady-state, the operating point for the power grid is calculated using a loadflow study.
5: At $k = 0^-$, a disturbance enters the grid, which is subsequently detected by all local clouds.
6: At $k = 0$, i.e. when the estimated state $\hat{\mathbf{x}}_\kappa(0)$ is assumed to be statistically close to the actual state $\mathbf{x}_\kappa(0)$, all local clouds send their estimated states to the CCO, thereby providing CCO with the full state vector $\hat{\mathbf{x}}_0$.
7: Following the control design steps provided in Sections 3–6, the CCO informs the local clouds to set-up distributed MPC controllers C_i, $\forall i = 1, \dots, r$.
8: For all utility areas $\kappa = 1, \dots, M$, the control loop is then iterated as follows, for $k \geq 0$.
9: **while** any local cloud detects significant oscillations in $\hat{\mathbf{x}}_\kappa$ **do**
10: States $\hat{\mathbf{x}}_\kappa(k)$ are distributed among the controllers according to (19) using wide-area communication links, as shown in Fig. 2(a) for the 5-machine example system.
11: Using (21)–(26), every dMPC controller C_i solves the problem $\mathcal{P}_i$, and then sends its control inputs to generators according to (18), as shown in Fig. 2(b).
12: Advance the control time-step $k \leftarrow k + 1$.
13: **end while**
14: All wide-area links are terminated, and the local clouds continue monitoring the steady-state state-estimates $\hat{\mathbf{x}}_\kappa$.

relaxed, leading to a denser topology until (29) is satisfied. In the worst case, this can result in all-to-all communication, where all controllers solve a centralized MPC problem. This situation, however, rarely arises in a practical WAC problem. As will be seen in simulations, more than 70% sparsity can be retained without destabilizing the system. Also, note that (29) is a sufficient condition, not necessary. Hence, in reality one may be able to achieve closed-loop stability with a much sparser controller than the one stipulated by Theorem 1.

7. Simulations

The 48-machine, 140-bus Northeast Power Coordinating Council (NPCC) nonlinear power system model (Rogers, 2012) is used to verify the control design, shown in Fig. 3. All generators are modeled using transient models with static exciters. Transformers are attached to all generator buses, and the system is open-loop stable. The system is divided into six utility areas based on electrical distances. Fig. 3 shows these areas with various background colors.

The system is linearized around its loadflow operating point. Since inter-area oscillation signal frequencies lie in the (0.1–2) Hz range for large power systems (Kundur, 1994), the discretized system can only be sampled with a minimum Nyquist frequency of 4 Hz to capture all inter-area modes. It is noted that $T = 0.1$ s (10 Hz) is chosen for discretizing the system.

7.1. State estimation

State estimation for the generator dynamics is implemented following the three-step procedure described in Section 2. The area-wise OPP problem (2) is solved for all $\kappa = 1, \dots, 6$, where the cost of installing PMUs is assumed to be unity for all buses. Locations for 39 PMUs are identified to assure observability of all generator buses. These buses are highlighted in red color in Fig. 3. Voltage, current, and their phase angle measurements are recorded from these buses. The measurement noise is assumed to be zero-mean Gaussian noise. The noise variance values are obtained from the study in Brown, Biswal, Brahma, Ranade, and Cao (2016), where a signal-to-noise ratio of 45 dB was concluded to be a good approximation for PMU data. This data is used to estimate the phasor currents and voltages at the generator buses by solving (5). Next, decentralized UKFs are used to estimate generator states with (6). State estimation results for generator 1, in open-loop, are shown in Fig. 5. The results are seen to be consistent with the ones reported in Singh and Pal (2014).

7.2. Post-disturbance modal analysis

The three scenarios considered for post-disturbance analysis on the NPCC model are:

(i) *Case Study I:* The system is perturbed with a three-phase fault on the transmission line connection buses 10–11. Starting the simulation in steady-state at $t = 0$ s, the fault is applied at 1.1 s, which is then cleared at 1.2 s at bus 10, and at 1.25 s at bus 11.
(ii) *Case Study II:* System is perturbed with a three-phase fault on the transmission line connecting buses 45–46. The fault is applied at 1.1 s, cleared at 1.2 s at bus 45, and at 1.3 s at bus 46.
(iii) *Case Study III:* System is perturbed with a three-phase fault on the transmission line connecting buses 119–120. The fault is applied at 1.1 s, cleared at 1.3 s at bus 119, and at 1.45 s at bus 120.

Note that the duration of the fault for Case Study I is smaller compared to other events. Since the eastern part of the power network is only connected via two buses (buses 29 and 35) to the rest of the grid, and due to the brief duration of this fault, it can be seen as a relatively 'localized' disturbance as compared to the other two events which occur on critical buses for longer durations. Once the fault is cleared at the remote end of the faulted line, the estimated post-disturbance system state $\hat{\mathbf{x}}_0$ is used to construct the MP matrix whose elements are shown pictorially in Fig. 4(a)–(c). The residues for these different events can clearly be seen to be different from each other. Hence, it is clear that different sets of generators are influencing different sets of inter-area modes depending on the magnitude and location of the fault.

7.3. Distributed control design

For brevity, control design steps are provided with respect to Case Study I only. Control designs for Case Studies II and III are done in a similar manner and their results are summarized in Table 1.

From the residues shown in Fig. 4(a), $\mu = 1.03$ is calculated for the MP matrix. Two modal areas are then constructed as $\mathcal{A}_1 = \{G_1, \dots, G_9\}$ and $\mathcal{A}_2 = \{G_{11}, G_{12}, G_{14}\}$, highlighted in Fig. 3 with dotted boundaries. It is noted that for this particular disturbance, only 12 out of 48 generators are influential in the dominant inter-area modes. The remaining 36 generators do not need to participate in wide-area control. Since for this case the intersecting sets between the non-overlapping modal areas are empty, $P_i = \mathcal{A}_i$, $\forall i = 1, 2$. Design of $r = 2$ distributed controllers is done for the two modal areas using the SDFT frequency windows (in

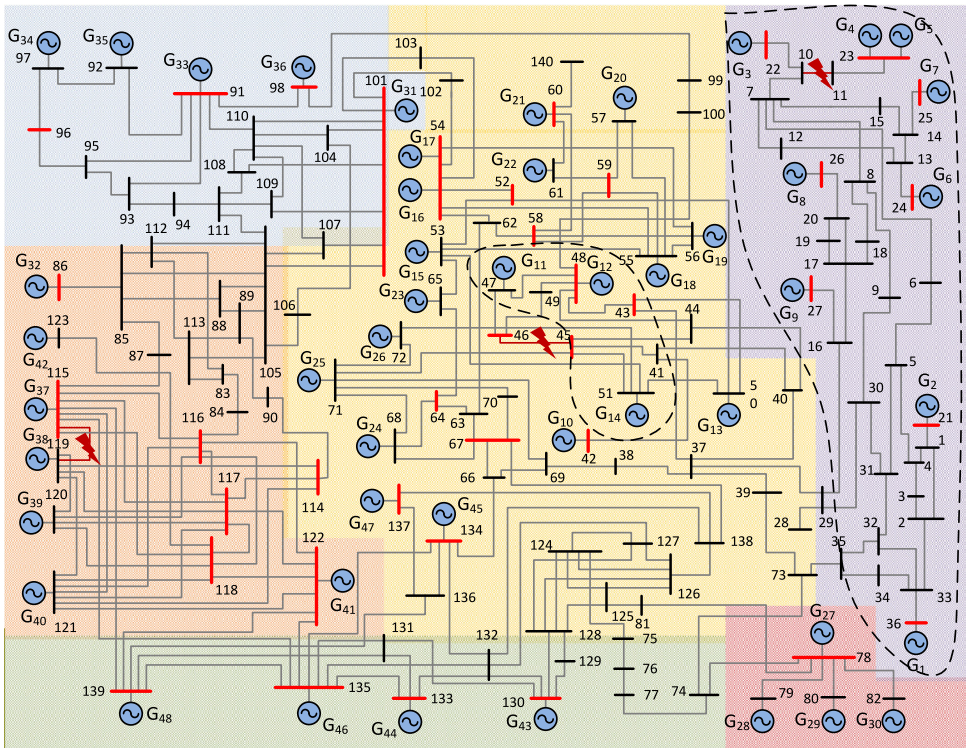

Fig. 3. The one-line diagram of the NPCC model shows the utility areas in various background colors. The PMU buses identified by solving the OPP problem (2) are highlighted in red color. Also shown are the three faults considered for the three case studies at lines connecting buses 10–11, 45–46 and 119–120. Modal areas for Case Study I are also shown, enclosed in dotted boundaries. (For interpretation of the references to color in this figure legend, the reader is referred to the web version of this article.)

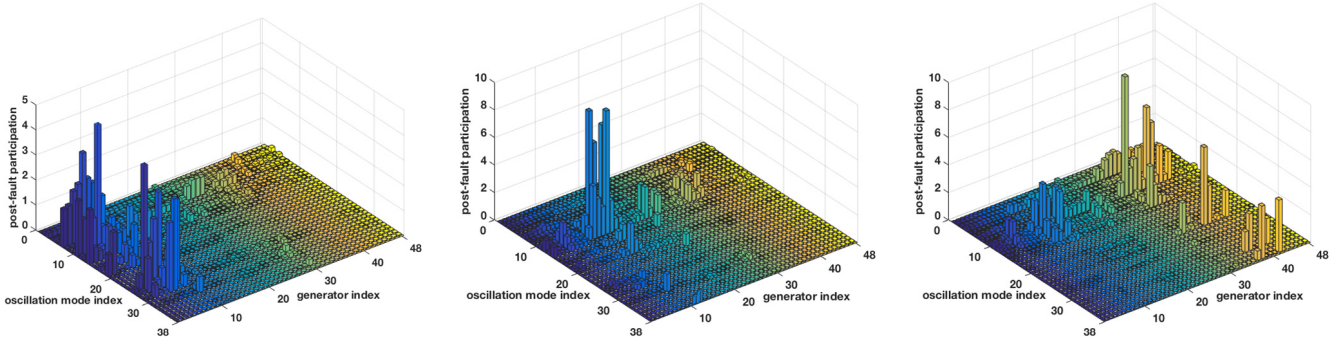

Fig. 4. MP matrices are shown for the three case studies in subfigures (a), (b) and (c) respectively. x- and y-axis represent generator and oscillation mode indices respectively, and z-axis represents modal residues. 38 oscillation modes are chosen such that these modes all have frequencies less than 1.5 Hz, and damping factors less than 0.3.

Table 1
dMPC simulation results for all case studies.

Case study	Fault location & duration	Open-loop dominant modes	No. of controllers	List of influential generators, and their assignments to controllers C_i	SDFT Windows (in Hz)	Perf. loss Index: ξ	Sparsity Index: θ	Optim. times (ms)
I	Line 10–11 for 0.15 s	$-0.038 \pm 3.8j$, $-0.419 \pm 6.5j$	2	$C_1^d = \{G_1, \ldots, G_9\}$ $C_2^d = \{G_{11}, G_{12}, G_{14}\}$ $C_1^u = C_1^d$, $C_2^u = C_2^d$	[0.53, 0.73], [0.86, 1.2]	0.121	0.250	50 (C_1), 10 (C_2)
II	Line 45–46 for 0.20 s	$-0.449 \pm 5.6j$, $-0.482 \pm 8.8j$	1	$C_1^d = \{G_{10}, \ldots, G_{17}, G_{33}, \ldots, G_{36}\}$ $C_1^u = C_1^d$	[0.95, 1.05], [1.35, 1.5] (2 windows)	0.328	0.250	80 (C_1)
III	Line 119–120 for 0.35 s	$-0.419 \pm 6.5j$, $-0.449 \pm 5.7j$	3	$C_1^d = \{G_{11}, G_{32}, \ldots, G_{38}\}$ $C_2^d = \{G_{11}, G_{12}, G_{14}, G_{33}\}$ $C_3^d = C_1^d \cup C_2^d$ $C_1^u = C_1^d - G_{11}$, $C_2^u = C_2^d - G_{11}$, $C_3^u = G_{11}$	[0.85, 0.95], [0.95, 1.05], [0.85, 1.05]	0.356	0.271	50 (C_1), 12 (C_2), 10 (C_3)

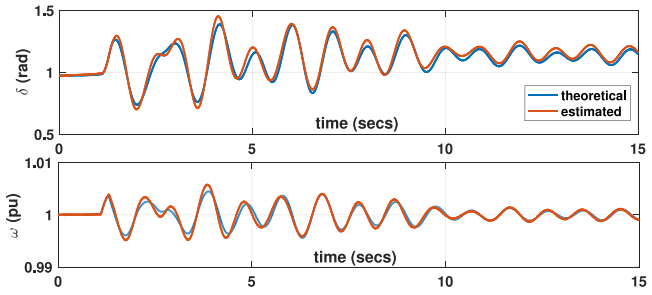

Fig. 5. Dynamic state estimation for the electromechanical states (δ and ω) of Gen. 1 with the decentralized UKF.

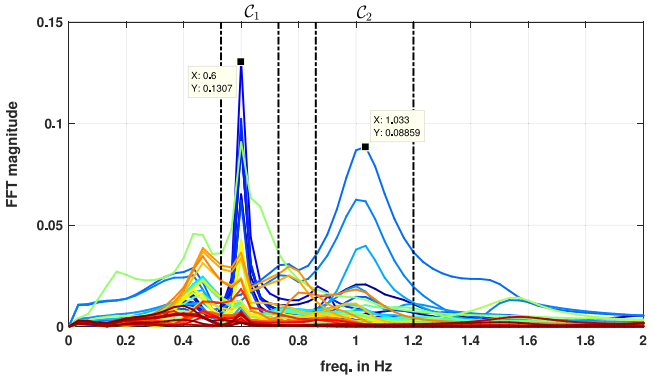

Fig. 6. Open-loop frequency response for all rotor speeds. SDFT windows for control design are highlighted.

Hz): $[0.53, 0.73]$ for $\mathcal{C}_1$ and $[0.86, 1.2]$ for $\mathcal{C}_2$. The open-loop frequency response for all rotor speeds is shown in Fig. 6. The windows are chosen by the CCO from the predicted open-loop frequency response. The input constraints enforced on the control signals are $-0.1 \leq u_i(t) \leq 0.1$, $\forall t > 0$, allowing for a maximum of 10% supplementary control effort in the excitation voltage. The optimization problem $\mathcal{P}_i$ in (25) is solved for the two controllers, with control weightings $\mathbb{R}_1 = \mathbb{R}_2 = \text{diag}(0.1, \ldots, 0.1)$ for less emphasis on the magnitude of control inputs. Additionally, $\mathbb{S}_1 = \mathbb{S}_2 = \text{diag}(0.01, \ldots, 0.01)$ to obtain a less conservative control policy. The prediction horizon is chosen as $N = 100$ keeping in mind the trade-off for unmeasured dynamics and SDFT resolution, as discussed in Remark 2. The control horizon is kept small for lower execution times at $N_c = 10$. The optimization toolbox in Matlab is used to solve the constrained QP (25) with the *interior-point convex* algorithm.

7.4. Closed-loop results

Fig. 7(a)–(b) show the rotor speed output for the generators 7 and 8, in open- and closed-loop. Closed-loop results are shown for both a centralized MPC implementation and the dMPC implementation. The centralized MPC receives state estimates of all 48 generators as feedback, and send control inputs to all 48 generators, and solves a single optimization problem at every time-step. In Fig. 7(a)–(b) it is seen that the dMPC performs close to the optimal centralized performance. Fig. 7(c) shows the comparison between the centralized MPC and the dMPC control input voltages, for both generators 7 and 8. As shown, the control voltages lie in the constraint set $[-0.1, 0.1]$.

A comparison of open-loop versus dMPC closed-loop electrical power outputs for selected generators is shown in Fig. 8. It can be clearly seen that the dMPC controller suppresses the oscillation amplitudes successfully for power output of all generators, even the ones not included in the control design. From the closed-loop frequency responses, it is observed that the dominant mode 1 (around 0.6 Hz) show a 40.2% reduction in FFT peak, and dominant mode 2 (around 1 Hz) show a 14.6% reduction. It is also observed that the frequency of the two dominant modes are almost same in open- and closed-loop.

Average controller optimization times are reported in Table 1, and for the considered case studies, observed to be less than the sampling time of 0.1 s. The optimization times increase with increasing the control horizon N_c and also with increasing the number of generators to be controlled with a single controller. For systems with even larger number of generators per controller, the optimization times can scale up rapidly. In such a case, priorities can be given to only those generators with the highest modal residues in oscillations, or faster computational resources can be provided to the local clouds. It is observed that a longer control horizon does not result in a significant improvement in performance and hence is kept small. For the centralized MPC controller, the average optimization time is observed to be 0.3 s, which is larger than the considered sampling time of 0.1 s. All simulations are performed on a 3.8 GHz quad-core Intel i7 processor with 16 GB RAM.

7.5. Performance vs. sparsity

To evaluate the trade-off between closed-loop performance and sparsity, a performance metric is defined as:

$$\mathcal{J} = \frac{1}{T_{ss}} \sum_{i=1}^{m} \sum_{k=1}^{T_{ss}} |y_i(k) - 1|^2, \tag{30}$$

where T_{ss} is the maximum settling time for all outputs, and y_i is the rotor speed of the ith generator, with a steady-state per unit value of 1. Let the open-loop cost, closed-loop centralized MPC cost, and the dMPC closed-loop cost be denoted by $\mathcal{J}^{ol}$, $\mathcal{J}^{cent}$ and $\mathcal{J}^{dmpc}$, respectively. $\mathcal{J}^{ol}$ is calculated from the same expression as (30), but when all generator

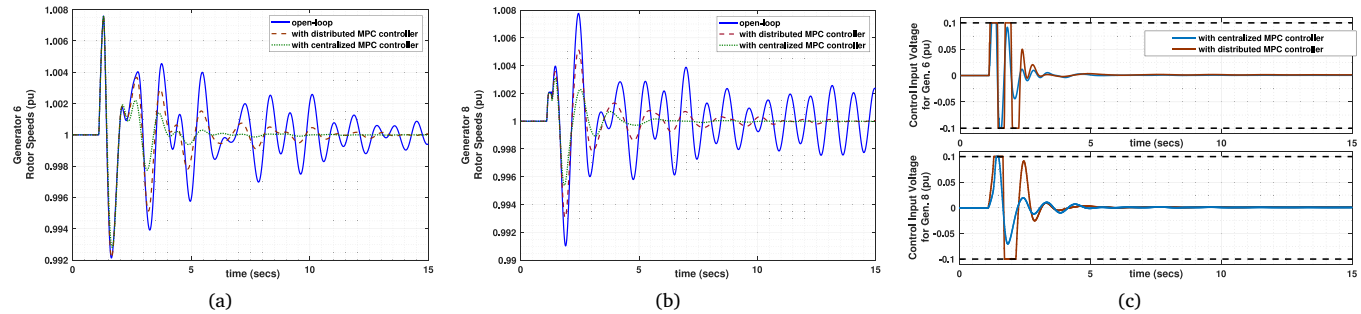

Fig. 7. Subfigure (a) and (b) shows the comparison of rotor speeds for generators 6 and 8 respectively, for the three cases of open-loop, closed-loop with dMPC controller and closed-loop with a centralized MPC controller. Subfigure (c) shows the comparison of control input voltages for generator actuators 6 and 8 respectively, for the two cases of dMPC controller and a centralized MPC controller.

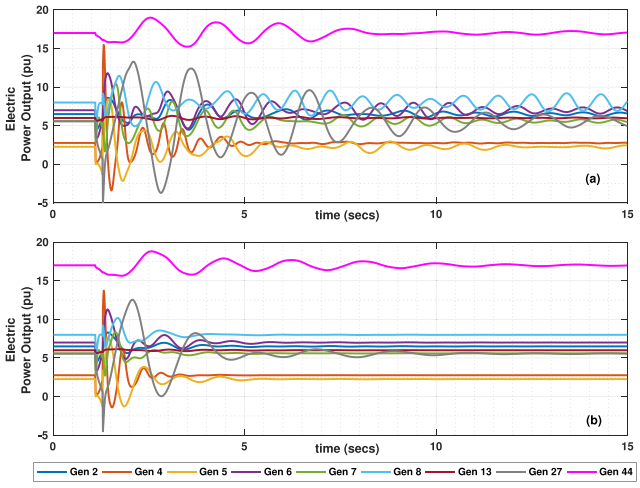

Fig. 8. (a) Open-loop vs. (b) dMPC closed-loop comparison is shown for electrical power outputs, in p.u., of all generator buses.

outputs y_i, $\forall i = 1, \ldots, m$ are in open-loop, i.e. no supplementary MPC control. The dMPC *performance loss index* is then defined as:

$$\xi = \frac{\mathcal{J}^{dmpc} - \mathcal{J}^{cent}}{\mathcal{J}^{ol} - \mathcal{J}^{cent}}. \tag{31}$$

Note that (31) normalizes the dMPC cost between $[0, 1]$ with 0 representing the optimal centralized cost, and 1 representing the open-loop cost. The closer ξ is to 0, the better is the dMPC performance. A *sparsity index* is also defined as the ratio between the number of unidirectional communication links required by the dMPC controller, to that required by the centralized MPC. Since a centralized MPC will essentially require communication with all generators, the number of required links will be $2m$. Hence the sparsity index is given by:

$$\theta = \frac{1}{2m} \sum_{i=1}^{r} [\text{card}(C_i^d) + \text{card}(C_i^u) + \phi_i], \tag{32}$$

where $\theta \in [0, 1]$, and ϕ_i is the number of controller-to-controller communication links needed due to possible overlapping modal areas. The closer θ is to zero, more is the sparsity (θ to be exactly 0, however, has no physical meaning in this case as that would mean that there is no dMPC controller).

Table 1 provides a summary of main results for the three case studies listed in Section 7.2. Since the fault in Case Study I is a 'localized' disturbance, a sparsity level of 75% is achieved (as compared to a centralized controller) for this event using two controllers. The performance loss index is also lowest for this case study since the effect of generators outside the identified modal areas is minimal, as a result of which the unmeasured generator dynamics are close to zero. This clearly shows the advantage of designing the proposed controller online after the fault happens instead of an offline controller that may be agnostic to the localized nature of the fault. Case Studies II and III also show an acceptable trade-off between performance and sparsity. The level of sparsity and performance with Case Study III is lower than the other two case studies due to the longer duration of fault resulting in overlapping modal areas, i.e. multiple generators participating substantially in excitation of same dominant inter-area modes. This necessitates the design of a third controller C_3 as listed in Table 1.

8. Conclusions

A distributed MPC design is presented for damping inter-area oscillations in a large power system network. A set of dominant inter-area modes, resulting from a major disturbance in the network, are first identified. Generators which have highest contribution to these modes are then identified to form the communication topology for distributed control. Energy content of the dominant modes is extracted from the output open-loop frequency spectrum using the SDFT method. A dMPC problem is then solved for each distributed controller, under communication and actuation constraints. Simulations performed on the NPCC model show effectiveness of the control design by successfully eliminating sustained low-frequency oscillations, while also saving on both communication links and computation times when compared to a centralized control implementation.

Acknowledgments

The work of the second author was partly supported by the US National Science Foundation under grants ECCS 1054394 and ECCS 1544871. The work of the third author was supported in part by the *BuildingControls* project funded by the European Commission (H2020-MSCA-IF-2015, grant no. 708984).

References

Alessio, A., & Bemporad, A. (2007). Decentralized model predictive control of constrained linear systems. In *European control conference* (pp. 2813–2818). IEEE.

Annaswamy, A. M., Hussain, A., Chakrabortty, A., & Cvetkovic, M. (2016). Foundations of infrastructure CPS. In *American control conference* (pp. 2649–2664).

Azad, S. P., Iravani, R., & Tate, J. E. (2013). Damping inter-area oscillations based on a model predictive control (MPC) HVDC supplementary controller. *IEEE Transactions on Power Systems*, *28*(3), 3174–3183.

Boukarim, G. E., Wang, S., Chow, J. H., Taranto, G. N., & Martins, N. (2000). A comparison of classical, robust, and decentralized control designs for multiple power system stabilizers. *IEEE Transactions on Power Systems*, *15*(4), 1287–1292.

Brown, M., Biswal, M., Brahma, S., Ranade, S. J., & Cao, H. (2016). Characterizing and quantifying noise in PMU data. In *Power and energy society general meeting, 2016* (pp. 1–5). IEEE.

Camponogara, E., Jia, D., Krogh, B., & Talukdar, S. (2002). Distributed model predictive control. *IEEE Control Systems*, *22*(1), 44–52.

Chakrabortty, A., & Khargonekar, P. P. (2013). Introduction to wide-area control of power systems. In *American control conference* (pp. 6758–6770). IEEE.

Chaudhuri, B., & Pal, B. (2004). Robust damping of multiple swing modes employing global stabilizing signals with a TCSC. *IEEE Transactions on Power Systems*, *19*(1), 499–506.

Christofides, P. D., Scattolini, R., de la Pena, D. M., & Liu, J. (2013). Distributed model predictive control: A tutorial review and future research directions. *Computers & Chemical Engineering*, *51*, 21–41.

Dörfler, F., Jovanovic, M. R., Chertkov, M., & Bullo, F. (2014). Sparsity-promoting optimal wide-area control of power networks. *IEEE Transactions on Power Systems*, *29*(5), 2281–2291.

Franze, G., & Tedesco, F. (2011). Constrained load/frequency control problems in networked multi-area power systems. *Journal of the Franklin Institute*, *348*(5), 832–852.

Gomez-Exposito, A., Abur, A., Rousseaux, P., de la Villa Jaen, A., & Gomez-Quiles, C. (2011). On the use of PMUs in power system state estimation. In *Proc. 17th power systems computation conference*, vol. 22 (p. 26).

Jain, A., Biyik, E., & Chakrabortty, A. (2015). A model predictive control design for selective modal damping in power systems. In *American control conference, 2015* (pp. 4314–4319). IEEE.

Jain, A., Chakrabortty, A., & Biyik, E. (2017). An online structurally constrained LQR design for damping oscillations in power system networks. In *American control conference* (pp. 2093–2098). IEEE.

Kundur, P. (1994). *Power system stability and control, vol. 7*. New York: McGraw-Hill.

Larsen, E. V., Sanchez-Gasca, J. J., & Chow, J. H. (1995). Concepts for design of FACTS controllers to damp power swings. *IEEE Transactions on Power Systems*, *10*(2), 948–956.

Maciejowski, J. M. (2002). *Predictive control: with constraints*. Pearson education.

Mc Namara, P., Negenborn, R. R., De Schutter, B., & Lightbody, G. (2013). Weight optimisation for iterative distributed model predictive control applied to power networks. *Engineering Applications of Artificial Intelligence*, *26*(1), 532–543.

Mohamed, T., Bevrani, H., Hassan, A., & Hiyama, T. (2011). Decentralized model predictive based load frequency control in an interconnected power system. *Energy Conversion and Management*, *52*(2), 1208–1214.

Negenborn, R. (2007). *Multi-agent model predictive control with applications to power networks* (Ph.D. thesis), TU Delft, Delft University of Technology.

Noroozian, M., Ghandhari, M., Andersson, G., Gronquist, J., & Hiskens, I. (2001). A robust control strategy for shunt and series reactive compensators to damp electromechanical oscillations. *IEEE Transactions on Power Delivery*, *16*(4), 812–817.

Pérez-Arriaga, I. J., Verghese, G. C., & Schweppe, F. C. (1982). Selective modal analysis with applications to electric power systems, Part I: Heuristic introduction. *IEEE Transactions on Power Apparatus and Systems*, (9), 3117–3125.

Rogers, G. (2012). *Power system oscillations*. Springer Science & Business Media.

Sauer, P. W., & Pai, M. (1997). Power system dynamics and stability. *Urbana*, *51*, 61801.

Singh, A. K., & Pal, B. C. (2014). Decentralized dynamic state estimation in power systems using unscented transformation. *IEEE Transactions on Power Systems*, *29*(2), 794–804.

Ulbig, A., Arnold, M., Chatzivasileiadis, S., & Andersson, G. (2011). Framework for multiple time-scale cascaded MPC application in power systems. *IFAC Proceedings Volumes*, *44*(1), 10472–10480.

Vazquez, S., Leon, J. I., Franquelo, L. G., Rodriguez, J., Young, H. A., Marquez, A., et al. (2014). Model predictive control: A review of its applications in power electronics. *IEEE Industrial Electronics Magazine*, *8*(1), 16–31.

Venkat, A. N., Hiskens, I. A., Rawlings, J. B., & Wright, S. J. (2008). Distributed MPC strategies with application to power system automatic generation control. *IEEE Transactions on Control Systems Technology*, *16*(6), 1192–1206.

Ye, H., & Liu, Y. (2013). Design of model predictive controllers for adaptive damping of inter-area oscillations. *International Journal of Electrical Power & Energy Systems*, *45*(1), 509–518.

Zhou, M., Centeno, V. A., Thorp, J. S., & Phadke, A. G. (2006). An alternative for including phasor measurements in state estimators. *IEEE Transactions on Power Systems*, *21*(4), 1930–1937.

Zolotas, A. C., Chaudhuri, B., Jaimoukha, I. M., & Korba, P. (2007). A study on LQG/LTR control for damping inter-area oscillations in power systems. *IEEE Transactions on Control Systems Technology*, *15*(1), 151–160.